*Int. J. Heat Mass Transfer.* Vol. 32, No. 8, pp. 1401–1411, 1989
Printed in Great Britain

0017–9310/89 $3.00 + 0.00
Pergamon Press plc

# Experimental data processing by means of 'asymptotic coordinates'

A. D. POLYANIN, V. A. ALVARES-SUARES, V. V. DIL'MAN and YU. S. RYAZANTSEV

Institute for Problems in Mechanics, U.S.S.R. Academy of Sciences, 117526, Moscow, U.S.S.R.

(*Received* 23 *January* 1987)

**Abstract**—A new simple method for processing experimental data is suggested which allows one, in many cases, to reveal universal relations in different fields of science and technology. The method also makes it possible to effectively model and forecast qualitatively similar phenomena and processes that occur under identical conditions. A number of concrete examples are considered of the suggested method of application to the analysis of some experimental results obtained when studying different processes of convective heat and mass transfer, chemical technology and hydrodynamics.

## 1. INTRODUCTION. OBJECTIVE. SOME EXPLANATIONS

GENERALLY, it is recommended that experimental data be processed using corresponding dimensionless parameters (such as Reynolds, Peclet, Damköhler, Marangoni numbers and others) [1–3]. This paper will show that for the purpose of generality it is much more preferable in many cases to process the final results of experimental studies in special 'asymptotic coordinates' similar to those used in refs. [4–9] to derive and improve various approximate relations.

In what follows, it will be assumed for the sake of definiteness that there is some unknown quantity $F$ which depends on two dimensionless parameters $p$ and $q$ ($0 \leqslant p, q < \infty$). For the conditions pertaining to the experiment the parameter $q$ will be assigned certain values, $q = q_1, q_2, \ldots$, and $F$ will be measured as a function of $p$ (i.e. a series of curves will be plotted in the $p$–$F$ plane for different values of $q$). Let the shape of the curves in the $p$–$F$ plane be qualitatively identical (see, e.g. Figs. 1(a), 2(a), 2(d), and 3).

In the overwhelming majority of cases it is the practice to analyze experimental data directly from the curves presented in the $p$–$F$ plane (the intervals of monotonicity in variation of $F$ with $p$ and $q$ are determined; comparison with other theoretical and experimental data is made, etc.). It should be noted that few studies are now available that suggest the approximate analytical relation $F = F(p, q)$ which would satisfactorily fit experimental results. (Here it is implied that the relation $F = F(p, q)$ is derived only by considering the set of curves in the $p$–$F$ plane without resorting to other additional information.)

As a rule, such a superficial analysis makes it possible to reveal only the simplest (often trivial) laws governing the process or phenomenon studied. Out of view, in this case, are more important general trends which are characteristic of the whole class of qualitatively similar phenomena and processes and which can be established only by analysing experimental results properly and in detail.

The presentation of the main principles of such a detailed analysis and classification of typical experimental curves of the simplest form which are frequently encountered in chemical technology, macrokinetics, hydrodynamics, power engineering and other fields of science and technology, is the concern of this paper.

The central part in this new method for investigating experimental data is occupied by the detailed study of the qualitative behaviour of curves in the $p$–$F$ plane in some specific limiting cases (usually when $p \to 0$ and $p \to \infty$). This analysis yields the form of new 'asymptotic coordinates' with the aid of which test data should be processed. In many cases the 'asymptotic coordinates' allow the complex two-dimensional experimental surface studied, $F = F(p, q)$, in a three-dimensional space to be described by several much simpler plane curves.

The method suggested has a number of advantages over traditional techniques of experimental data processing. Namely, the representation of the two-dimensional surface sought, $F = F(p, q)$, by plane curves allows the construction of an approximate analytical formula directly (due to the fact that the interpolation of plane curves offers no difficulties and can be performed, for example, by the method of least squares) which rather accurately describes experimental results. (Note, that usually simple approximate formulae are more convenient for interpolation and practical use than tables and graphs.) Another, even more important fact is that a plane curve plotted in 'asymptotic coordinates' often has a universal character and is good for describing a whole class of qualitatively analogous processes and phenomena occurring under identical conditions (for example, being properly converted into 'asymptotic coordinates' a

## NOMENCLATURE

| | | | |
|---|---|---|---|
| $B$ | electric tension | $v_g$ | gas velocity |
| $d_p$ | diameter of naphthalene particle | $v_m$ | minimum rate of fluidization. |
| $d_n$ | diameter of glass spheres | | |
| $h$ | height of asperity | | |
| $I$ | current intensity | Greek symbols | |
| $k$ | mass transfer coefficient | $\delta$ | thickness of viscous sublayer |
| $Re$ | Reynolds number | $\eta$ | viscosity. |

number of the basic parameters of the flow and of heat and mass transfer in circular and square cross-section tubes will fall on the same experimental curve). It is very helpful to use this fact for modelling and forecasting different processes, the direct experimental study of which is very costly or difficult to realize.

Before moving on directly to the classification of the most common experimental curves and to the description of corresponding 'asymptotic coordinates' it is useful to consider the following simple example which illustrates very well all the basic features of the proposed rather general scheme of experimental data processing. Let there be a series of curves on the $p$–$F$ plane consisting of rectilinear sections inclined at different angles to the $p$-axis over the interval $[0, p_*]$ and of matched straight lines parallel to the $p$-axis, with $p_* \leqslant p$ (Fig. 1(a)). (Note that this form is typical of the fluidization curves for a very polydispersed oxidation catalyst, that pass through the coordinate origin (see Fig. III.17, p. 159 of ref. [10]).)

The dependence of the function on the second parameter $q$ will be plotted first for two characteristic values of the parameter $p$ (0 and $p_*$). This yields the functions

$$\varphi = \varphi(q) \equiv F(0, q), \quad \psi = \psi(q) \equiv F(p_*, q) \tag{1}$$

which are presented schematically in Fig. 1(b).

Direct verification will easily show that on substitution of the function $F$ by the new auxiliary function $f = f(p, q)$ with the following formula:

$$f = \frac{F - \varphi}{\psi - \varphi} \equiv \frac{F(p, q) - F(0, q)}{F(p_*, q) - F(0, q)} \tag{2}$$

and using the normalized variable $\xi = p/p_*$ instead of the coordinate $p$, then all the curves in Fig. 1(a) will converge into one curve passing through the points $(0, 0)$ and $(1, 1)$ as shown in Fig. 1(c).

Thus, it is shown that in the given case the set of curves in the $p$–$F$ plane in Fig. 1(a) can be described by three plane curves shown in Figs. 1(b) and (c).

Using the graphs in Fig. 1(b), it is not difficult to construct an approximate analytical dependence of

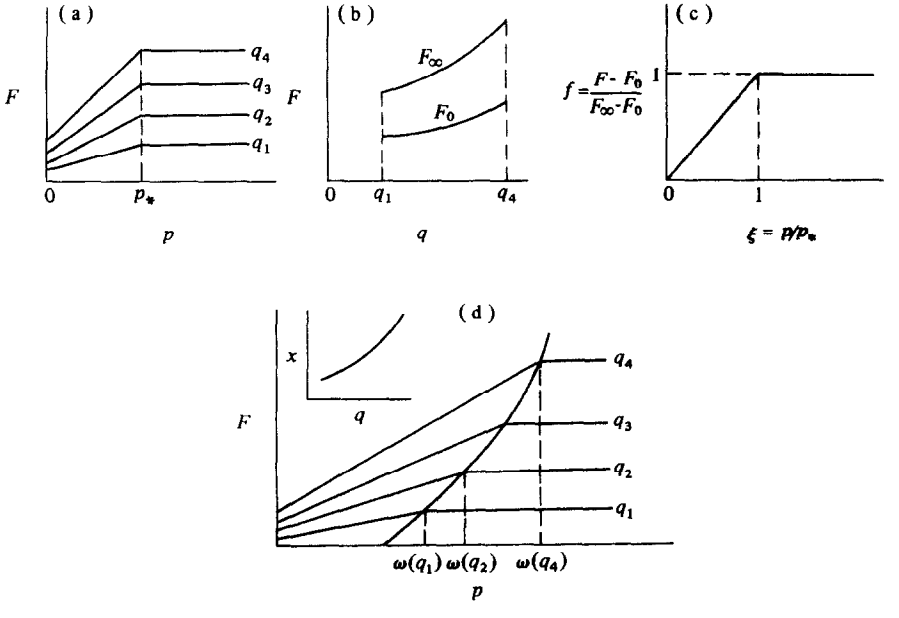


FIG. 1.

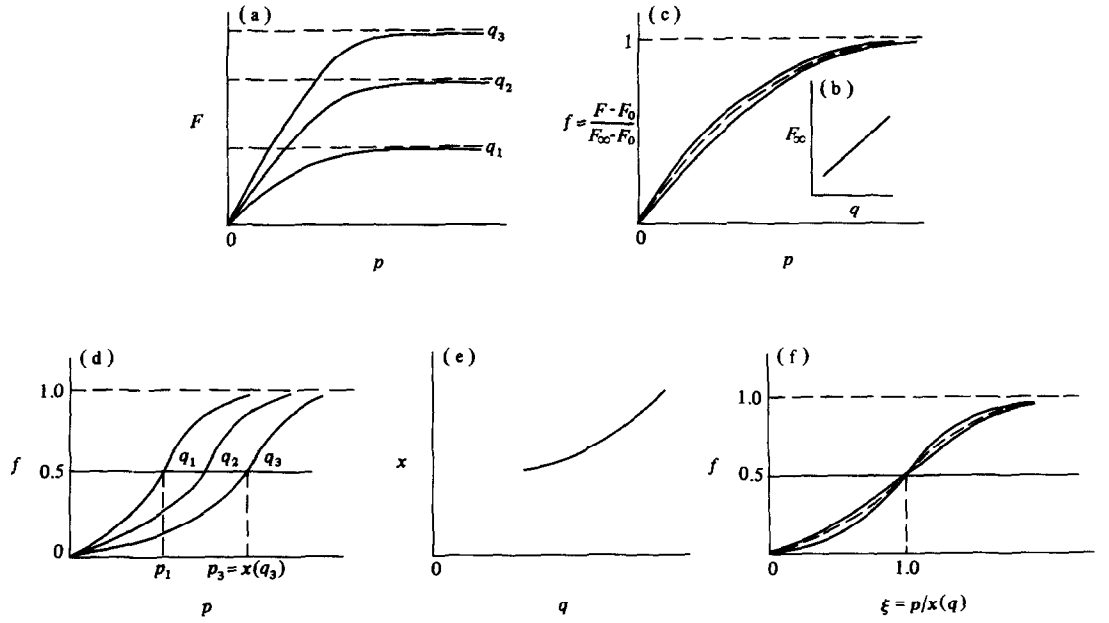


FIG. 2.

the auxiliary functions $\varphi$ and $\psi$ on the parameter $q$. This can be done quite differently by many techniques if only the uncertainty of the approximate expressions used does not exceed the error of the experimental data. (Specific examples of the construction of such approximate formulae will be considered later in Sections 3 and 4.) Note that the main criteria for the quality of approximate relations are the simplicity and compactness of the appropriate analytical expressions.

Now, taking into account the fact that the function $f$ has, according to Fig. 1(c), the form

$$f = \begin{cases} p/p_* & \text{as } 0 \leqslant p \leqslant p_* \\ 1 & \text{as } p_* \leqslant p \end{cases} \tag{3}$$

and making use of equation (2), the following analytical expression for the initial function $F$ is obtained:

$$F(p,q) = \begin{cases} \varphi(q) + [\psi(q) - \varphi(q)](p/p_*), & 0 \leqslant p \leqslant p_* \\ \psi(q), & p_* \leqslant p. \end{cases}$$

It is important to emphasize for the subsequent discussion that the auxiliary functions shown in Figs. 1(b) and (c) play quite different roles in the description of the experimental series of curves in Fig. 1(a), namely the most important characteristic here is equation (3) shown in Fig. 1(c). In fact, the curve in Fig. 1(c) completely retains the structure and specific features of the initial series of curves in the $p$–$F$ plane (see Fig. 1(a)). Moreover, it does not change at all (in other words remains invariant) when other series of curves of qualitatively similar character are considered. Therefore, the plane curve in Fig. 1(c) contains much more factual information and has a considerably wider range of applicability than the initial experimental series of curves in Fig. 1(a) (in this sense the curve in Fig. 1(c) can be said to possess universality).

The auxiliary functions $\varphi$ and $\psi$ in Fig. 1(b) play the role of 'boundary' conditions for the series of curves in Fig. 1(a); they will differ for other series of curves of qualitatively similar character (therefore, they do not possess universality).

Henceforth, the new variables of type (2) will be called the 'asymptotic coordinates'. This name is very convenient because it reminds us that these variables are introduced with the aid of limiting (i.e. asymp-

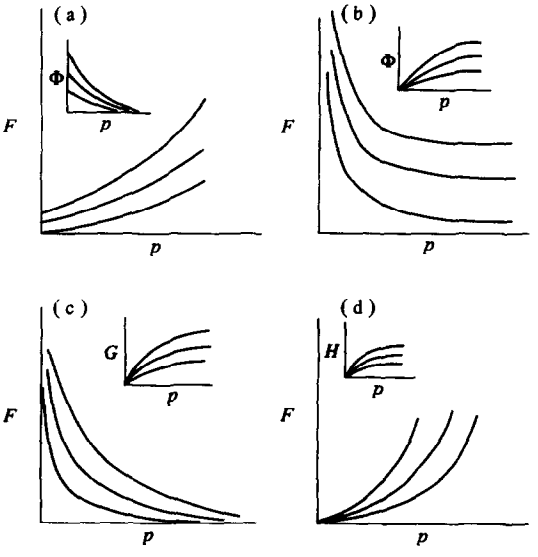


FIG. 3.

totic) values of the initial quantity $F$ (in the given case with $p \to 0$ and $p \to \infty$).

Consider now the somewhat more complex model situation presented in Fig. 1(d), namely all of the experimental curves consist of two rectilinear segments, but the boundary of the region where the function $F$ depends only on $q$ and does not depend on $p$ is curvilinear (in Fig. 1(a) this boundary has the form of a straight line which is prescribed by the value $p = p_*$).

It will be shown that simple stretching along the coordinate $p$ can bring this series of curves to the previous simple case shown in Fig. 1(a). Introduce a new auxiliary function $x = x(y)$ which is constructed in the following way: at the prescribed value of $q$ the magnitude of the function $x$ is determined by the value of the $p$-coordinate for the point of joining of the rectilinear segments in Fig. 1(d).

Now, replacing $p$ by the new coordinate

$$\xi = p/x(q) \tag{4}$$

will give the situation which is shown in Fig. 1(a) at $p_* = 1$ and which was analysed in detail above.

Note that in the given case the series of experimental curves in Fig. 1(d) can be described by four plane curves (it is convenient to plot three auxiliary functions $x$, $\varphi$, $\psi$ in one figure).

In many cases the basic properties of the model examples considered can be also extended to a more complex series of experimental data occurring in practice.

## 2. CLASSIFICATION OF THE EXPERIMENTAL CURVES OF THE SIMPLEST FORM

Now, some typical series of curves, which are frequently encountered in experimental works, will be described.

It will be assumed that all of the curves in the $p$–$F$ plane that correspond to different values of the second independent parameter $q$, increase (or decrease) monotonously with the parameter $p (0 \leqslant p,\ q < \infty)$. As before, it is also assumed that these curves have qualitatively similar form. The classification of this kind of experimental curves will be based on the study of the limiting (asymptotic) behaviour of these curves in the $p$–$F$ plane at great and small $p$s.

### 2.1. *Case* 1

First, consider a very common situation characterized by the conditions

$$\lim_{p \to 0} F = F_0(q) \neq \infty, \quad \lim_{p \to \infty} F = F_\infty(q) \neq \infty. \tag{5}$$

For simplicity, here the functions $\varphi$ and $\psi$ (see Section 1) were more conveniently designated by $F_0$ and $F_\infty$ which emphasize the limiting character of these auxiliary functions.

A typical series of experimental curves that satisfy conditions (5) when $\partial F/\partial p \geqslant 0$ is presented in Fig. 2(a). Figure 2(b) shows the plot of the functions $F_\infty = F_\infty(q)$ constructed from the data of Fig. 2(a).

By analogy with the results obtained earlier for the model example in Section 1, the function $F$ will be replaced here by a new auxiliary function $f = f(p, q)$ according to the formula

$$f = \frac{F - F_0}{F_\infty - F_0} \equiv \frac{F(p,q) - F(0,q)}{F(\infty, q) - F(0,q)}. \tag{6}$$

In Fig. 2(c) the dependence of $f$ on the parameters $p$ and $q$ is shown.

It is seen that at any values of the parameter $q$ the function $f$ possesses the following useful properties:

$$f = 0 \quad \text{at} \quad p = 0; \quad f = 1 \quad \text{at} \quad p = \infty.$$

Therefore, it turns out frequently that the curves in the $p$–$f$ plane (plotted from the data of Fig. 2(a)) adjoin each other rather tightly (see Fig. 2(c)). In such cases it is convenient to use an approximate relation for the function $f$ (dashed line in Fig. 2(c)). In other words, here the sought-after complex two-dimensional surface $F = F(p, q)$ in a three-dimensional space can be described by only three plane curves which are presented in Figs. 2(b) and (c). This technique of describing experimental results is adequate for the analysis of a series of curves that approach the asymptote at approximately the same value of the parameter $p$.

When, with $p \to \infty$, the function $F$ attains its limiting value in a more complex way, the variable $p$ should be appropriately extended in the $p$–$F$ plane simultaneously so that the curves could approach the asymptote (this technique was used in Section 1 in the second model example shown in Fig. 1(d)). This gives a more simple case which has been considered above.

Another possible way for experimental data processing consists of the following. Changing to the new coordinate (6) in the $p$–$f$ plane gives the situation shown in Fig. 2(d). Let $p_i \equiv x(q_i)$ be the coordinate of the point at which the curve 'numbered' $q_i$ intersects with the straight line parallel to the $p$-axis and which is prescribed by the equation $f = 1/2$. The values of these coordinates for different $q_i$s (where $i = 1, 2, \ldots$) determine the function

$$x = x(q), \quad |f(x(q), q) \equiv 1/2|$$

shown in Fig. 2(d).

Now, in lieu of $p$ introduce a new stretched variable

$$\xi = p/x(q) \tag{7}$$

and plot the curves presented in Fig. 2(d) in the $\xi$–$f$ plane (Fig. 2(f)). It is seen that all the experimental curves for any value of $q$ possess the limiting properties

$$\lim_{\xi \to 0} f = 0 \quad \text{and} \quad \lim_{\xi \to \infty} f = 1$$

and, besides, pass through the same point with the coordinates $\xi = 1$, $f = 1/2$. The last-mentioned important fact (which was not the case for the curves

in the $p$–$f$ plane) leads usually to the situation when the experimental curves in the $\xi$–$f$ plane are rather tightly 'pressed' to each other and can be approximately substituted by the sole line (the dashed line in Fig. 2(f)).

Making use of the results of Section 1, it is possible to show that any limited (in $F$) family of poorly deformed curves in the $p$–$F$ plane is transformed by the above method to the series of curves which occupy a narrow region in the $p$–$f$ (or $\xi$–$f$) plane and, consequently, it is well approximated by one plane curve.

Note that in a number of cases the approximate relation in Fig. 2(c) can be rather accurately described by the following simple formulae:

$$f = \frac{p^n}{a+p^n} \tag{8a}$$

or

$$f = 1-\exp(-bp^m) \tag{8b}$$

where the parameters $a$, $b$, $n$, $m$ are calculated from experimental data. It should also be borne in mind that it is sometimes convenient to present the equation of the curve in Fig. 2(c) in the form of the implicit expression

$$p = \frac{aF}{(1-F)^n} \tag{8c}$$

where $a$ and $n$ are appropriate numerical parameters.

For the function $f$ to be described approximately, use can also be made of more complex three-term expressions which result from the right-hand sides of equations (8a) and (8b) being raised to some power $l$.

It will now be shown in which way some experimental curves of the other type can be analysed by reducing them by simple transformations to case 1.

2.2. *Case* 2

Consider a series of experimental curves which satisfy the conditions

$$\lim_{p\to 0} F = F_0(q) \neq \infty, \quad \lim_{p\to\infty} F = \infty \ (F_0 \not\equiv 0). \tag{9}$$

The typical behaviour of the corresponding curves in the $p$–$F$ plane is shown in Fig. 3(a).

This situation can be most simply analysed when $F$ is replaced by a new variable

$$\Phi = 1/F. \tag{10}$$

This enables the situation to be reduced to the first case at $\Phi_\infty = 0$.

2.3. *Case* 3

Let the following conditions take place:

$$\lim_{p\to 0} F = \infty, \quad \lim_{p\to\infty} F = F_\infty(q) \neq \infty \quad (F_\infty \not\equiv 0). \tag{11}$$

A typical series of experimental curves which possess the properties of equation (10) is shown in Fig. 3(b).

Changing from the function $F$ to the new variable $\Phi = 1/F$ yields again the first case considered above at $\Phi_0 = 0$.

2.4. *Case* 4

Analyse now the situation which is shown in Fig. 3(c) and which is realized under the conditions

$$\lim_{p\to 0} F = \infty, \quad \lim_{p\to\infty} F = 0. \tag{12}$$

The introduction of the new auxiliary function $G$ instead of $F$ by

$$G = \frac{1}{F+1} \tag{13}$$

enables this situation to be reduced to case 1.

2.5. *Case* 5

The satisfaction of the conditions

$$\lim_{p\to 0} F = 0, \quad \lim_{p\to\infty} F = \infty \tag{14}$$

gives a series of curves shown in Fig. 3(d).

The use of the new variable

$$H = \frac{F}{F+1} \tag{15}$$

instead of $F$ again allows one to come to case 1 studied earlier.

There are also other, more complex situations which can be considered in a similar way (the dependence of $F$ on the parameters $p$ and $q$ must not be necessarily monotonous). In particular, it is not difficult to show that the proposed method always makes it possible to reveal a self-similar character of experimental results (if it takes place, of course). Moreover, with the use of this method it is possible to completely describe the following, more general functional relationship:

$$F(p,q) = \alpha(q)+\beta(q)f\left(\frac{p}{x(q)}\right) \tag{16}$$

where $\alpha$, $\beta$, $x$, $f$ are arbitrary functions.

Making use of the above method of investigation, we will now analyse some specific experimental data of chemical technology and hydrodynamics.

## 3. CONCRETE EXAMPLES OF EXPERIMENTAL DATA PROCESSING: TURBULENCE AND FLUIDIZED BED

3.1. *Electrochemical method for turbulence measurements in liquids*

In refs. [11, 12] an electrochemical method is described which was used for measuring velocity and concentration fluctuations in turbulent liquid flow.

The working element was a nickel electrode, on the surface of which chemical reactions take place. The

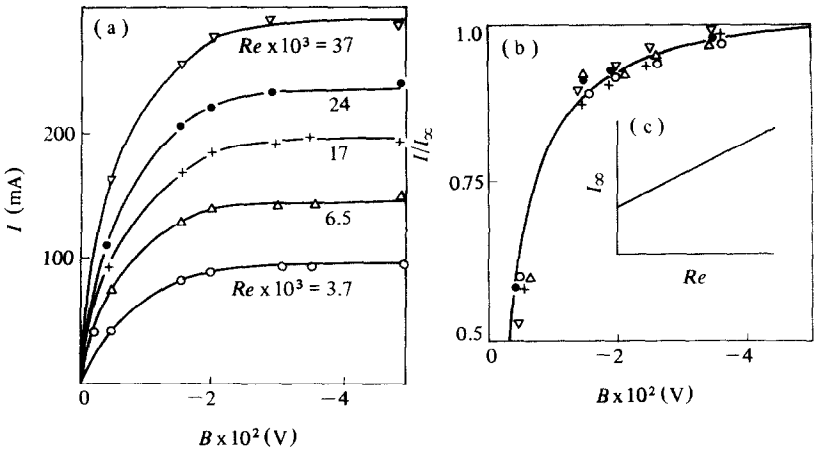


FIG. 4.

voltage applied can reduce the concentration of reacting components on the electrode surface to zero. Such an electrode can be interpreted as an analogue of a thermoanemometer which operates in the mode of a constant temperature (in the sense that the concentration on the electrode surface is maintained constant while the current in the circuit is dependent on the rate of mass transfer).

In Fig. 4(a) the dependence of the current $I$ variation with the applied (negative) voltage $B$ is shown at different Reynolds numbers $Re$ [11, 12].

Using the familiar formulae [12], it is possible to calculate the coefficient of mass exchange between the ferricyanide ions in the solution and on the cathode. This, in turn, enables the mean and fluctuational components of the turbulent flow velocity gradient to be determined (these flow characteristics are linearly related to the coefficient of mass transfer).

All the curves in Fig. 4(a) emerge from the coordinate origin, i.e. the condition $I_0 = I(Re, 0) = 0$ is fulfilled. Therefore, in accordance with the results of Section 2, that the obtained experimental results can be more conveniently interpreted, the relationship $I/I_\infty = I(Re, B)/I(Re, \infty)$ should be used as a new variable.

Figure 4(b) shows the dependence of the quantity $I/I_\infty$ on the parameter $B$ at different Reynolds numbers. It is seen that all the experimental data (see Fig. 4(a)) are well described by the sole universal relation. It follows from Fig. 4(c) that the limiting value of the saturation current $I_\infty$ depends linearly on the Reynolds number $Re$.

Thus, all the test data of refs. [11, 12] are completely described by two simple plane curves presented in Figs. 4(b) and (c).

An approximate analytical expression for the normalized saturation current is constructed on the basis of equation (8a) at $n = 3/2$. As a result, the following relation is obtained:

$$\frac{I}{I_\infty} = \frac{(B/B_*)^{3/2}}{1+(B/B_*)^{3/2}}, \quad B_* = 0.003b. \tag{17}$$

The straight line in Fig. 4(c) is described by the expression

$$I_\infty = \alpha Re + \beta \tag{18}$$

where $\alpha = 0.007$ mA and $\beta = 70$ mA.

Equations (17) and (18) form an analytical representation of the experimental results in Fig. 4(a).

### 3.2. *Mass transfer of particles in a fluidized bed*

In ref. [13] mass transfer is experimentally studied from a naphthalene particle of diameter $d_p$ ($2 < d_p < 20$ mm) freely moving in a fluidized bed composed of glass spheres of diameter $d_n$ ($100 < d_n < 700$ $\mu$m). Fluidization was achieved by a flow of heated air at the temperature of 65°C. The mass transfer coefficient was determined by a change in the mass of the naphthalene particle as a function of two characteristic dimensions—$d_p$ and $d_n$. The airflow velocity was twice the minimum rate of fluidization.

This experiment is of great practical importance, since it models the burning of coal particles in reactors.

Figure 5(a) shows the dependence of the measured mass transfer coefficient $K$ on the naphthalene particle diameter $d_p$ at different sizes of particles, in the fluidized layer, $d_n$.

As the parameter $d_p \to 0$, the curves in Fig. 5(a) become infinite. Therefore, in the given case by changing from the function $K(d_n, d_p)$ to the function $\Phi = K_{\min}(d_n, d_p)/K(d_n, d_p)$ we again come to the case described in Section 2 (see Fig. 3(b)).

Figure 5(b) presents the dependence of the function $\Phi$ on the size of naphthalene particles and the solid phase of the fluidized bed plotted from the data of Fig. 5(a). It can be easily verified that for all $d_n$s all

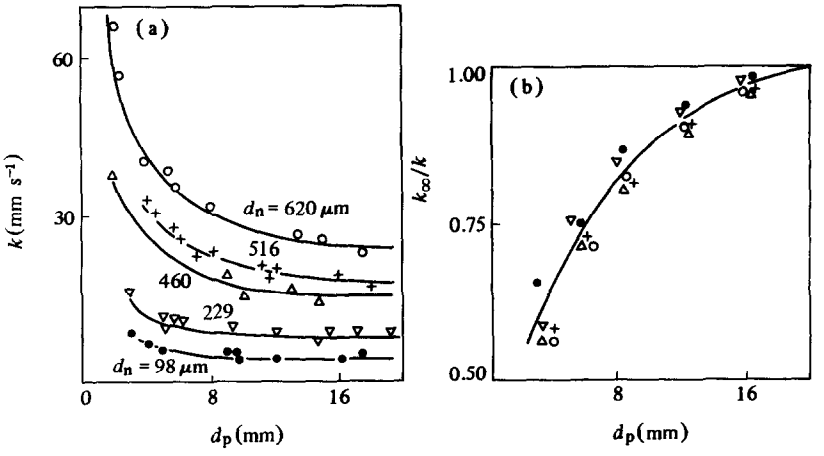


FIG. 5.

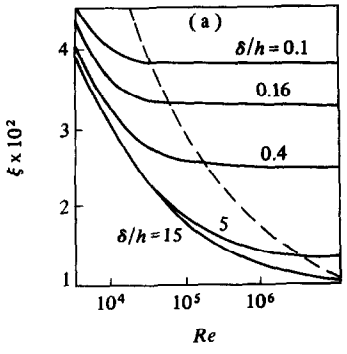


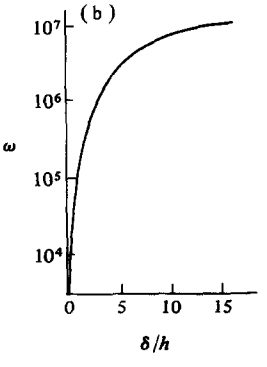


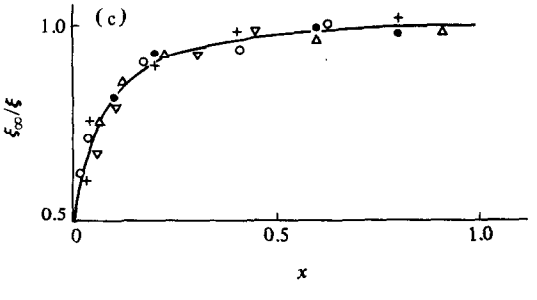


FIG. 6.

the experimental points fall on a single curve (shown by a solid line).

Variation of the normalized mass transfer coefficient with the particle diameter (see Fig. 5(b)), can be described, accurate up to 5%, by a formula similar to equation (8b)

$$\frac{K_{\min}}{K} = 1 - \exp\left\{-0.38\left(\frac{d_p}{d_*}\right)^{3/2}\right\} \qquad (19)$$

where $d_* = 2$ mm.

### 3.3. *Hydraulic resistance of rough tubes*

It is known that the hydraulic resistance of rough tubes tends to be the same as that of smooth tubes till the height of a viscous sublayer $\delta$ exceeds the height of roughness asperities $h$. As soon as the asperities turn out to be in the turbulent region of the flow, they start to generate vortices and viscous friction ceases to noticeably affect the flow velocity profile in the bulk of the liquid. At large enough Reynolds numbers $Re$ the resistance coefficient in rough tubes is independent of this criterion.

Under operating conditions the roughness of tubes is very nonuniform and therefore the transition to the region, where $\xi$ is independent of $Re$, is gradual.

Figure 6(a) shows the dependence of the resistance coefficient of industrial steel tubes $\xi$ on $Re$ at different ratios $\delta/h$ which is given in ref. [14].

Figure 6(b) presents the auxiliary function $\omega = \omega(\delta/h)$ which was plotted in the following way. At the given value of the parameter $\delta/h$ the value of the function $\omega$ is determined by the value of $Re$ — the coordinates of the points at which the curves in Fig. 6(a) pass to a straight section (dashed line in Fig. 6(a)).

Using the technique described in Sections 1 and 2, introduce a new coordinate $x = Re/\omega(\delta/h)$ by equation (4). In Fig. 6(c) the dependence of the reciprocal coefficient of the hydraulic resistance $\xi_{\min}/\xi$ on $x$ is

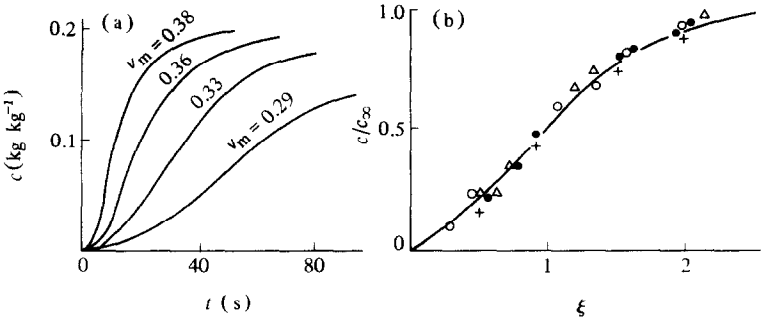


FIG. 7.

plotted. It is seen that for any values of $\delta$, $h$, $Re$ and $\xi$ the test data 'fall' with a high degree of accuracy on one curve in the $x$–$\xi_{min}/\xi$ plane.

The two plane curves presented in Figs. 6(b) and (c) give a full description of the experimental results presented in ref. [14]. (Here and hereafter to economize on space, we do not present corresponding approximate analytical equations for the plane curves; they can be constructed, e.g. by appropriately selecting parameters in equations (8a) and (8b).)

### 3.4. *Distribution of particles and mixing in a centrifugal fluidized bed*

In ref. [15] experimental results were presented for a fluidized bed of glass beads. The experimental setup consisted of a cylindrical vessel which rotated around its vertical axis and the bottom of which was covered with white (80%) and red (20%) glass particles. The diameter of particles was 0.44 mm. The distribution of particles, prescribed at the initial time instant, was achieved by cardboard partitions which were removed after the rotating vessel attained the set angular velocity of rotation $v_r$. An airflow was fed through the vessel bottom at different velocities. The weight concentration of particles of different colours near the vessel walls was measured by weighing the particles which got into standard traps in the upper lid of the cylinder.

The plots of concentration $C$ vs time $t$ at different values of the minimum rate of fluidization $v_m$ are given in Fig. 7(a). As is seen from the graphs presented, when $t \to \infty$ the curves attain the limiting value ($C = 0.20$) in a rather complicated manner (see also Fig. 2(d)). In this case let us extend the variable $t$ by the method described in Section 2 (case 3). Draw a straight line, parallel to the $t$-axis, which is prescribed by the equation $C = (1/2)$, and let $t$ be the coordinates of the points at which the curves $C = C(t, v_m)$ intersect with this line. The values of these coordinates for different $v_m$, determine the function $x = x(v_m)$.

Now introduce the extended variable $\xi = t/x(v_m)$ and represent the experimental curves given in Fig. 7(a) in the coordinates $f = C/C_\infty$, $\xi$ (Fig. 7(b)). By construction, the relations $f(0) = 0$, $f(1) = 1/2$, $f(\infty) = 1$ will be satisfied for the function $f$. It is seen that all the experimental data for any values of the parameter $v_m$, are 'tightly' pressed to each other and can be approximately substituted by the sole solid line in Fig. 7(b).

### 3.5. *Hydrodynamic characteristics of a three-phase fluidized bed*

Experiments on the study of hydrodynamic characteristics of a three-phase fluidized bed (gas–liquid–solid) were described in ref. [16]. The study was made in an attempt to investigate the dependence of the minimum rate of fluidization $v_m$ on the gas velocity $v_g$, density $\rho$ and on the size of solid particles $d$ and also on the liquid viscosity $\eta$. (The local concentrations of solid, liquid and gas phases were measured by the electrical conductivity method.)

Figure 8(a) gives an example of obtaining the minimum rate of fluidization $v_m$ as a function of the liquid viscosity $\eta$ and gas velocity $v_g$ at fixed values of $\rho$ and $d$. The experiments were conducted with glass particles of radius 2.3 mm and density $\rho = 2.24$ g cm$^{-2}$.

According to the procedure described in Section 2 (see case 1), making use of equation (6) and taking into account that $v_m(\infty, 0) = 0$ we shall introduce a new auxiliary function

$$f = 1 - \frac{v_m(v_g, \eta)}{v_m(0, \eta)}. \tag{20}$$

Figure 8(b) shows the dependence of the quantity $f$ on $v_g$ and $\eta$. It is seen that in this case too all the experimental data can be described by a single curve.

### 3.6. *Use of photochromic compounds in the experimental hydrodynamics*

In recent times, the method of hydrodynamic flow visualization based on the use of a photochromic indicator has been used to advantage. Directed radiation of a certain wavelength produces coloured tracks in a solution the lengths of which depend on the type of photochromic compound, its concentration, intensity of activating radiation and other parameters. The registration of track locations at successive time instants makes it possible to study the liquid flow structure around differently shaped bodies [17, 18].

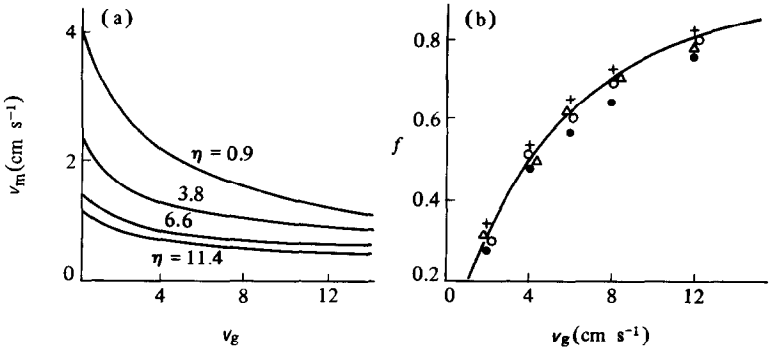


FIG. 8.

In ref. [18] the dependence of the length of a coloured track $l$ on the magnitude of the pulse laser radiation energy $E$ and the concentration of photochromic substance in a solution $C$ was studied. The experiments were conducted in a quartz cuvette filled with an aqueous solution of spiropyran 11 irradiated by a focused pulse laser at a wavelength $\lambda = 3473$ Å. The resulting coloured tracks in the liquid were photographed by a still camera.

In Fig. 9(a) the experimental dependence of the track length $l$ on the activating radiation energy $E$ is presented for four concentrations $C = 6\times10^{-4}$, $1.2\times10^{-4}$, $1.8\times10^{-4}$, $2.4\times10^{-4}$ g l$^{-1}$ (lines 1–4, respectively), which were determined by the photochromic substance to the solvent mass ratio. The laser enabled single pulses with an energy of $0.01 < E < 0.04$ J to be obtained. To elongate the coloured track, the multi-phase effect with maximum possible energy was exerted on the solution. The number of pulses in a series varied from 2 to 6. The time between separate pulses in the series amounted to $10^{-7}-10^{-6}$ s. In Figs. 9(a) and (b) the values $E = 0.08$, 0.12 and 0.16 J correspond to two-, three- and four-pulse activation of liquid.

It follows from the relations presented that an increase in the activation energy to the values greater than 0.12 J does not lead to a noticeable growth of the track length $l$, and, as $E$ grows, the length of the coloured track $l$ for each concentration $C$ tends to some limiting value $l_\infty$. (The quantity $l_\infty$ was taken to be the value $l$ at $E = 0.24$ J which corresponded to a six-pulse effect on the solution.) Therefore, when processing experimental data, it is expedient to change over to the normalized track length $l/l_\infty$.

In Fig. 9(b) the solid line presents the dependence of $l/l_\infty$ on $E$ constructed from the data of Fig. 9(a). It is seen that, irrespective of the concentration $C$, all the experimental points fall well on one universal curve. The dashed line corresponds to the results of the calculation by

$$\frac{l}{l_\infty} = 1 - \frac{E_*}{E}, \quad E = 0.01\,\text{J} \tag{21}$$

which represents well the experimental data.

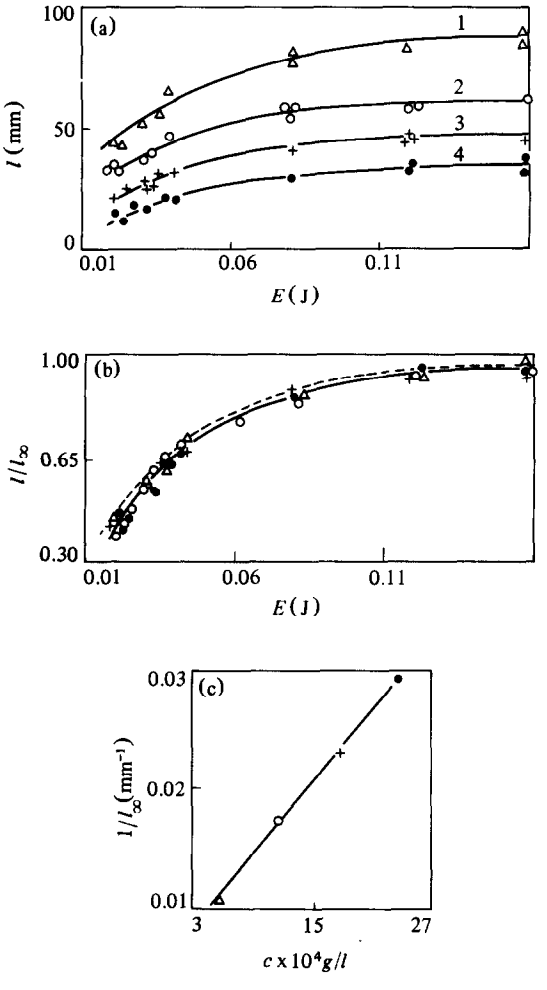


FIG. 9.

Figure 9(c) shows the dependence of the inverse quantity $1/l_\infty$ on the concentration $C$ obtained with the aid of Fig. 9(a). All the test points are located near the straight line, the equation of which can be written in the form

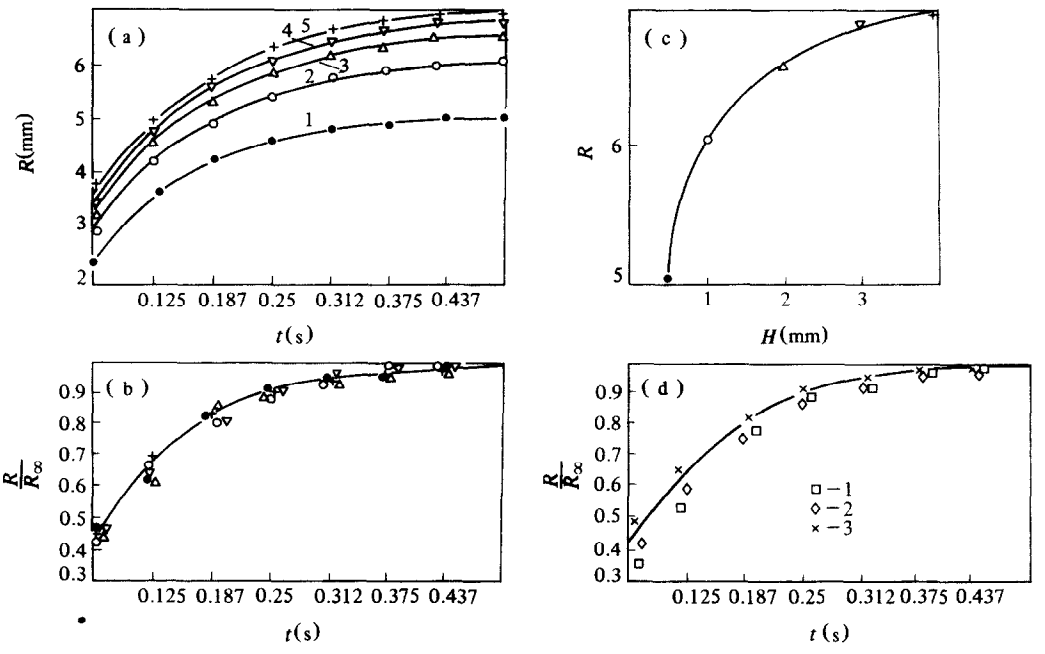


FIG. 10.

$$\frac{1}{l_\infty} = \alpha C + \beta \tag{22}$$

where $\alpha = 10\ \text{mm}^{-1}$ and $\beta = 0.005\ \text{mm}^{-1}$.

Thus, when the technique of photochromic visualization is used in hydrodynamic experiments for aqueous solutions of spiropyran 11 with the concentration $5 \times 10^{-4} < C < 3 \times 10^{-3}$ g $l^{-1}$, the length of the coloured track can be calculated from equations (21) and (22). It is to be expected that expressions (21) and (22) with other values of constants $E_*$, $\alpha$ and $\beta$ turn to be also suitable for calculations of the coloured track lengths in solutions of other photochromic substances with different solvents.

### 3.7. *Thermocapillary motion of liquid*

It is known that the presence of a temperature gradient on the liquid surface leads to the appearance of a gradient of surface tension forces and to the motion of liquid under the action of these forces (Marangoni effect). In ref. [19] data are given on the thermocapillary motion of liquid caused by local heating of the interphase surface by a pulse of ultraviolet radiation.

It was noted in experiments with alcoholic photochromic solutions that in the zone of liquid, through which colouring initiating radiation passed, there was an intensive radial motion on the liquid surface. This phenomenon is due to the fact that in the case of rather a strong irradiation a column of heated (and coloured) liquid is formed which is spread from the phase interface. The appearance of the temperature gradient gives rise to the radial, from the beam axis, flow of the liquid upper layer, and the colouring of the activated solution makes it possible to register this motion.

In the experiments, photographs of the spot spreading over the solution free surface in a round cuvette were made at successive time instants. The liquid layer height $H$, concentration of photochromic substance $C$ and the pulse laser radiation energy $E$ were varied. In Fig. 10(a) the dependence of the radius of spreading $R$ of the outer boundary of the coloured spot on the time $t$ and $C = 0.2$ g $l^{-1}$ and $E = 0.08$ J is shown. Curves 1–5 correspond to the liquid layer height $H = 0$, 5, 1, 2, 3, 4 mm (the spot was initiated in the centre of the round cuvette of radius 50 mm). It is seen that when $t \to \infty$ there exists a finite limiting value for the radius $R$ which depends on the height $H$. It should be noted that for $H > 4$ mm there is virtually no effect of the cuvette bottom (i.e. when $H > 4$ mm, the corresponding curves practically merge).

Passing to the dimensionless value $R/R_{\max}$, where $R_{\max}$ is taken to be the value of $R$ at the time instant $t = 1$ s, we shall obtain the relation shown in Fig. 10(b). It is seen that at any height of the liquid column $H$ all the test data fall well on a single curve (solid line in Fig. 10(a)). In Fig. 10(c) the dependence of $R$ on $H$ is shown.

It is important to emphasize that the radius of the coloured spot $R$ in an alcoholic solution was measured at different concentrations $C$ and energies $E$. Irrespective of these parameters, all the test data processed in the variables $R/R_\infty$ and $t$ are well described by the sole universal curve shown in Fig. 10(d). (It will be

recalled that the value of $R_\infty$ varies at different values of $H$ and $E$.) Curves 1–3 in Fig. 10(d) correspond to the values of $E = 0.025$, 0.05 and 0.08 J.

## REFERENCES


1. A. A. Gukhman, *Introduction into the Similarity Theory*. Izd. Vysshaya Shkola, Moscow (1963).
2. A. A. Gukhman, *Application of the Similarity Theory to the Study of Heat and Mass Transfer Processes*. Izd. Vysshaya Shkola, Moscow (1967).
3. L. I. Sedov, *Similarity and Dimensional Methods in Mechanics*. Izd. Nauka, Moscow (1981).
4. V. V. Dil'man and A. D. Polyanin, New approximate methods of chemical mechanics, *Dokl. Akad. Nauk SSSR* **271**(6), 1444–1448 (1983).
5. A. D. Polyanin and V. V. Dil'man, Formulae of higher factual information in chemical mechanics, *Dokl. Akad. Nauk SSSR* **277**(1), 150–153 (1984).
6. V. V. Dil'man and A. D. Polyanin, A method of asymptotic extrapolation in the problems of convective mass- and heat-transfer, *Teor. Osnovy Khim. Tekhnol.* **17**(4), 435–440 (1983).
7. A. D. Polyanin and V. V. Dil'man, Asymptotic interpolation in the problems of mass- and heat-transfer and hydrodynamics, *Teor. Osnovy Khim. Tekhnol.* **19**(1), 3–11 (1985).
8. A. D. Polyanin and V. V. Dil'man, New methods of the mass- and heat-transfer theory—I. The method of asymptotic correction and the method of model equations and analogies, *Int. J. Heat Mass Transfer* **28**, 25–43 (1985).
9. A. D. Polyanin and V. V. Dil'man, New methods of the mass- and heat-transfer theory—II. The methods of asymptotic interpolation and extrapolation, *Int. J. Heat Mass Transfer* **28**, 45–58 (1985).
10. M. E. Aerov and O. M. Todes, *Hydraulic and Thermal Principles of Operation of Stationary and Fluidized Granular-bed Apparatus*, Izd. Khimiya, Leningrad (1968).
11. J. E. Mitchell and R. J. Henratty, A study of turbulence at a wall using an electrochemical wall shear stress meter, *J. Fluid Mech.* **26**(1), 199–221 (1966).
12. W. Frost and T. H. Moulden, *Handbook of Turbulence*. Plenum Press, New York (1977).
13. W. Prins, T. P. Casteleijn, W. Draijer and W. P. Van Swaij, Mass transfer from a freely moving single sphere, *Chem. Engng Sci.* **40**(3), 481–497 (1985).
14. S. S. Kutateladze, *Fundamentals of the Heat Transfer Theory*. Atomizdat, Moscow (1979).
15. D. G. Kroger, G. Abdenour, E. K. Levi and J. C. Chen, Particle distribution and mixing in a centrifugal fluidized bed. In *Fluidization*, pp. 349–356. Plenum Press, New York (1980).
16. J. M. Begovich and J. S. Watson, Hydrodynamic characteristics of three-phase fluidized beds. In *Fluidization*, pp. 190–195, *Proc. 2nd Engng Foundation Conf.* University Press, Cambridge (1978).
17. V. A. Barachevskiy, V. F. Mandzhikov, Yu. S. Ryazantsev, Yu. P. Strokach and V. V. Yurechko, Photochromic method for the visualization of hydrodynamic flows, *Prikl. Mat. Tekh. Fiz.* No. 5, 73–76 (1984).
18. V. A. Alvares-Suares, A. D. Polyanin and Yu. S. Ryazantsev, Study of the laws governing the colouring of photochromic solutions used in experimental hydrodynamics, *Prikl. Mat. Tekh. Fiz.* No. 1, 12–15 (1987).
19. V. A. Alvares-Suares and Yu. S. Ryazantsev, On thermocapillary motion caused by local liquid heating by an ultraviolet pulse, *Prikl. Mat. Tekh. Fiz.* No. 6, 165–168 (1986).


## TRAITEMENT DES DONNEES EXPERIMENTALES PAR LES "COORDONNEES ASYMPTOTIQUES"


**Résumé**—On suggère une nouvelle méthode simple pour le traitement des données expérimentales qui donne, dans beaucoup de cas, les relations universelles dans différents domaines de la science et de la technologie. La méthode rend possible la modélisation effective et la prédiction quantitative des phénomènes similaires et des procédés qui se produisent dans des conditions identiques. On considère plusieurs exemples concrets d'application de la méthode à l'analyse de quelques résultats expérimentaux obtenus pour différents mécanismes de transfert de chaleur et de masse, de technologie chimique et d'hydrodynamique.


## MESSWERTVERARBEITUNG MIT HILFE "ASYMPTOTISCHER KOORDINATEN"


**Zusammenfassung**—Es wird ein neues, einfaches Verfahren zur Meßwertverarbeitung vorgestellt, mit dem in vielen Fällen die grundlegenden Zusammenhänge technischer und wissenschaftlicher Probleme dargestellt werden können. Das neue Verfahren ermöglicht eine wirksame Modellierung und Vorhersage quantitativ ähnlicher Vorgänge und Erscheinungen, die unter identischen Bedingungen ablaufen. Es wird eine Anzahl konkreter Beispiele geprüft, bei denen das vorgeschlagene Verfahren bei der Untersuchung von Meßwerten angewandt wird. Die Meßwerte wurden bei der Untersuchung konvektiver Wärme- und Stoffübertragungsvorgänge chemischer und hydrodynamischer Prozesse ermittelt.


## ОБРАБОТКА ЭКСПЕРИМЕНТАЛЬНЫХ ДАННЫХ С ПОМОЩЬЮ "АСИМПТОТИЧЕСКИХ КООРДИНАТ"


**Аннотация**—Предлагается новый простой способ обработки экспериментальных данных, позволяющий во многих случаях выявлять универсальные зависимости в различных областях науки и техники. Этот метод дает возможность также эффективно моделировать и заранее прогнозировать качественно аналогичные явления и процессы, протекающие в сходных условиях. Рассмотрен ряд конкретных примеров применения предложенного метода для анализа некоторых экспериментальных результатов, полученных при исследовании различных процессов конвективного массо- и теплопереноса, химической технологии и гидродинамики.